

Role of nonlinear dynamics in accelerated warming of Great Lakes

Sergey Kravtsov, Noriyuki Sugiyama and Paul Roebber

Abstract

In recent decades, the Laurentian Great Lakes have undergone rapid surface warming with the summertime trends substantially exceeding the warming rates of surrounding land. Warming of the deepest Lake Superior was the strongest, and that of the shallowest Lake Erie — the weakest of all lakes. We investigate the dynamics of accelerated lake warming in idealized coupled thermodynamic lake–ice–atmosphere models. These models are shown to exhibit, under identical seasonally varying forcing, multiple possible stable equilibrium cycles, or regimes, with different maximum summertime temperatures and varying degrees of wintertime ice cover. The simulated lake response to linear climate change in the presence of the atmospheric noise rationalizes the observed accelerated warming of the lakes, the correlation between wintertime ice cover and next summer’s lake-surface temperature, as well as higher warming trends of the (occasionally wintertime ice-covered) deep-lake vs. shallow-lake regions, in terms of the corresponding characteristics of the forced transitions between colder and warmer lake regimes. Since the regime behavior in the models considered arises due to nonlinear dynamics rooted in the ice–albedo feedback, this feedback is also the root cause of the accelerated lake warming simulated by these models.

1 Introduction

In recent decades, a large number of lakes all over the globe have been undergoing rapid increase in surface water temperature (Schneider et al. 2009; Schneider and Hook 2010; O’Reilly et al. 2015). Furthermore, many of the lakes exhibited summertime warming trends exceeding the globally averaged surface temperature trend over land. This is in sharp contrast with the observed oceanic surface warming, which was generally smaller than the warming over land (see, for example, Manabe et al. 1991; Sutton et al. 2007; Joshi et al. 2008; Joshi and Gregory 2008; Byrne and O’Gorman 2012, among others).

Despite that some of the ice-free lakes were exhibiting rapid warming (Schneider et al. 2009), the wintertime ice-covered lakes were found, on average, to warm significantly faster than the ice-free lakes (O’Reilly et al. 2015), at the rates also exceeding those of

Department of Mathematical Sciences, Atmospheric Sciences Group, University of Wisconsin-Milwaukee, Milwaukee, WI 53201, USA; E-mail: kravtsov@uwm.edu

ambient air temperatures. This accelerated warming appears to be associated with a variety of climatic drivers and, interestingly, depends on the lakes morphology, with the deepest lakes exhibiting the largest warming trends (Austin and Colman 2007; Hampton et al. 2008; Zhong et al. 2016). Among Great Lakes, for example, Lake Superior (the deepest) has the strongest, and Lake Erie (the shallowest) — the weakest surface warming trend (Austin and Colman 2007). This dependence of the warming rates on depth is also found within individual lakes (**Fig. 1**). Yet another interesting aspect of the Great Lakes' recent evolution, which also appears to depend on the depth of the lake, is an apparent discontinuous jump in the time series of their summertime surface temperature, lake's heat content, and some other lake properties at around 1997–98. This discontinuity was, once again, most pronounced in Lake Superior, and least pronounced in Lake Erie (Van Cleave et al. 2014; Gronewold et al. 2015; Zhong et al. 2016).

The dynamical causes of the accelerated warming of mid-latitude lakes are still a subject of debate. A combination of explanatory factors have been considered, such as increases in incoming shortwave radiation and air temperature (Arvola et al. 2010; Ackerman et al. 2013; Foster and Heidenger 2013; Fink et al. 2014; Gronewold et al. 2015), shorter lake-ice durations (Magnuson 2000), as well as an earlier onset and longer duration of the summer stratification (Austin and Colman 2007; Austin and Allen 2011; Piccolroaz et al. 2015; Zhong et al. 2016). Of the processes mentioned above, the direct response to surface air temperature trends appears to dominate the surface warming of small, shallow lakes (Toffolon et al. 2014), but other processes may be equally or more important in determining the response of deeper, larger lakes (Zhong et al. 2016).

Since the seasonal presence of lake-ice is clearly a factor characterizing the majority of the most rapidly warming lakes, the ice–albedo feedback has been suggested as a root dynamical cause of accelerated lake warming (Austin and Colman 2007). In support of this idea, Hanrahan et al. (2010) found a correlation between the amount of winter ice cover and the summer surface water temperature of Lake Michigan. By contrast, Vavrus et al. (1996), Gerbash et al. (2008) and Zhong et al. (2016) argue that the net influence of lake ice on the lake's response to ambient warming is limited due to compensation between ice–albedo and insulating effects of the ice.

Here we address the multi-faceted problem of the accelerated lake warming using an idealized lake–ice–atmosphere coupled model. The central result of this study is an identification of multiple stable equilibrium seasonal cycles of the lakes (hereafter, the lakes' regional climate regimes) in our coupled model. These nonlinear regimes occur throughout the range of model geometries we considered, from one-column lakes of uniform depth to three-column lakes mimicking the geometry of individual Great Lakes, and derive their existence from the lake-ice–albedo feedback. Global warming experiments with our coupled model rationalize many qualitative and quantitative aspects of the observed accelerated lake warming, including the dependence of the warming trends on lake depth, the association between wintertime ice cover and next summer's surface temperatures, and abrupt regional climate change associated with transitions between warm and cold lake-climate regimes.

2 Coupled lake–ice–atmosphere model

Adequately addressing dynamics of the Great Lakes’ regional climate variability requires faithful simulation of the lake/lake-ice seasonal cycle. Typically, lake temperatures remain vertically homogenous throughout a substantial portion of the spring and fall seasons, and the lakes become stratified in winter and summer (**Fig. 2**); the lake ice appears when lake-surface temperatures cool below 0°C. The previous formulations of the one-dimensional lake models (e.g., Hostetler and Bartlein 1990) exhibited substantial biases in the duration of both the stratified and lake-ice seasons of deep lakes (Martynov et al. 2010). We introduced improvements in the lake-model vertical mixing scheme to alleviate these biases and developed a coupled configuration of the model with an interactive atmosphere to address lakes’ regional climate change.

a) Model geometry and experimental set up. We considered an idealized lake that has n lake columns characterized by a variable time- and depth-dependent temperature. If $n = 1$, the lake has a uniform depth; we also considered the case with $n = 3$ to model the lakes with non-trivial bathymetry. The lake is surrounded by land and overlaid by two atmospheric layers (**Fig. 3**). Lake columns do not exchange heat horizontally, and we assume no heat transport through the bottom of the lake. The lake absorbs and emits radiation and exchanges heat with the lower atmospheric layer at the surface. The lower atmospheric layer, nominally the atmospheric boundary layer, is divided into parts whose boundaries coincide with those of lake columns or land; each part has a distinct variable temperature predicted by the coupled model equations, and we allow lateral heat transport between adjacent parts of this layer. On the other hand, the uppermost layer represents the lower free atmosphere and has a specified variable temperature $T_{a,u}$, which enters the formulation of the model’s forcing in both stationary and global-warming experiments (see below). The model behavior is a function of a number of free parameters. Two such parameters are the relative size of land surrounding the lake and the efficiency of heat transport within the atmospheric boundary layer; both parameters affect the magnitude of the lake’s simulated warming trend.

b) Lake model. The individual columns of the lake model are governed by the one-dimensional model formulation of Hostetler and Bartlein (1990), with empirical improvements in its so-called enhanced minimum diffusion scheme on top of the modifications suggested by Fang and Stephan (1998) and Bennington et al. (2014). These further modifications were designed to achieve better modeling of the lakes’ seasonal cycle, in particular in conjunction with the correct simulation of the onset date and duration of the summer stratification season, which is notoriously difficult to simulate in one-dimensional deep-lake models (see Martynov et al. 2010; Subin et al. 2012; Bennington et al. 2014; Zhong et al. 2016). Simulations with our modified uncoupled lake–lake-ice model driven by the observed variable atmospheric radiation, surface temperature and wind result in a fairly good match between the simulated lake temperatures (**Fig. 2**) and observations thereof (not shown here).

c) Ice model. The lake ice is simulated using one-dimensional thermodynamic sea-ice model of Semtner (1976) modified to exclude the effects of brine pockets and explicit

representation of the snow cover. To account for the latter, we instead set the surface albedo of the ice exceeding the 10-cm thickness to 0.45, which is between the typical ice and snow albedo; the surface albedo for the ice thickness h between 0 and 10 cm in our model changes linearly from 0.05 (open water value) to 0.45. For simplicity, we ignore the insulating effects of snow. The type of the ice model we used was also different depending on the ice thickness. In particular, we used what Semtner (1976) called the 0-layer model for the thin ice ($h \leq 10$ cm), and the four-layer ice model otherwise. We find that the multi-layer ice model leads to simulating a more realistic — shorter — ice-season duration compared to the 0-layer models described in Hostetler and Bartlein (1990), especially for deep lakes.

d) Atmospheric component, coupling and external forcing. An active atmospheric boundary layer is assumed to have zero heat capacity and is thus always balanced in terms of the incoming and outgoing heat fluxes, which include long-wave and short-wave radiation, sensible and latent heat exchange with the lake or ice — parameterized via bulk formulas, — as well as lateral diffusive heat transports between adjacent atmospheric columns. The external forcing in the model reflects the periodic seasonal dependence in the shortwave radiation SW (which is all transmitted through the atmosphere and absorbed by the lake or land), free-atmosphere temperature $T_{a,u}$ and surface wind speed u :

$$SW(t) = \overline{SW} + 125 \cos(2\pi(t - 172)/365), \quad (1)$$

$$T_{a,u}(t) = \bar{T} + 16 \cos(2\pi(t - 180)/365), \quad (2)$$

$$u(t) = 7.5 - 2.5 \cos(2\pi(t - 195)/365). \quad (3)$$

The units here are W m^{-2} for heat fluxes, $^{\circ}\text{C}$ for temperatures and m s^{-2} for wind speeds; time t is measured in days. The \overline{SW} and \bar{T} denote the annual-mean values of short-wave radiation and free-atmosphere temperature. The amplitude of $T_{a,u}(t)$ was chosen so that the simulated surface water temperature seasonal variation roughly matched that of Great Lakes. The seasonal variation of $u(t)$ was chosen based on the fact that the climatological surface wind speed over land surrounding the Great Lakes is roughly 5 or 6 m s^{-1} in winter and 3 or 4 m s^{-1} in summer, and that surface wind speed is generally greater over the Great Lakes than over land. For the single-column lake experiments, we set $\overline{SW} = 175 \text{ W m}^{-2}$, which is comparable to the amount of downward shortwave radiation in the Great Lakes region. The phase shift in the formula of downward shortwave radiation was chosen so that the radiation reaches its maximum value on June 21-st, but the phase shifts in the formulas of the other two quantities are somewhat arbitrary, except to ensure that the free-atmosphere temperature reaches its maximum value in summer and surface wind speed in winter.

Below, we will extensively analyze the numerical experiments in which the free-atmosphere annual-mean temperature \bar{T} exhibits a linear trend of ± 0.04 $^{\circ}\text{C}$ per year and/or quasi-periodic or stochastic interannual variability.

3 Multiple regimes in lakes of uniform depth

a) Hysteresis behavior. To identify multiple stable equilibrium seasonal cycles of the lakes, we computed the hysteresis curves in the phase plane of the lake's maximum (summertime) surface water temperature and the concurrent annual-mean free-atmosphere temperature (**Fig. 4**). We first used a steady (seasonally periodic) forcing with the low value of the annual-mean free-atmosphere temperature \bar{T} to reach a seasonally varying lake equilibrium characterized by abundant wintertime ice cover and low summertime surface temperatures. We then added a linear trend of $+0.04^\circ\text{C}$ per year to \bar{T} and followed the evolution of the lake's seasonal cycle (red curves in Fig. 4). This trend is slow enough that the resulting forcing is essentially quasi-stationary, and leads to the lake seasonal cycle initially exhibiting gradual changes, with progressively less wintertime ice cover (not shown) and progressively warmer summertime temperature. This behavior ends when the lake abruptly transitions, at some value of the free-atmosphere temperature T_{\max} , to the wintertime ice-free state (not shown), which has a higher maximum (summertime) lake-surface temperature. Upon this transition, the ice-free warm state resumes gradual linear changes under a continued free-atmosphere temperature trend. Starting from the rightmost part of the hysteresis diagrams in Fig. 4, we now reverse the sign of the annual-mean free-atmosphere temperature trend, making it equal to -0.04°C per year (blue curves). The ice-free state gradually cools down until it reaches another threshold value of the free-atmosphere temperature T_{\min} and transitions abruptly back to the cold regime with substantial wintertime lake ice cover. Further slow decrease of the \bar{T} forcing results in the quasi-stationary and linear lake-temperature changes along the original line of the experiment with the warming trend.

In the range of the annual-mean upper air temperature forcing between T_{\min} and T_{\max} , the seasonally varying warm and cold climate regimes described above coexist. The occurrence of multiple equilibrium seasonal cycles of the lakes crucially depends on the lake-ice-albedo feedback — we obtained no evidence of multiple regimes in any simulations in which the ice-surface albedo was made equal to that of water (green curves).

b) Multiple regimes in one-column lakes of different depths. Different panels of Fig. 6 correspond to the hysteresis diagrams computed for the one-column coupled lake models of different depths. We observe that: (i) the multiple regimes of deeper lakes occur at colder values of \bar{T} forcing compared to the multiple regimes of shallower lakes; (ii) the range $T_{\max} - T_{\min}$ of \bar{T} in which the two regimes exist simultaneously is larger for deeper lakes; and (iii) the difference in the maximum summertime temperature between the two regimes is also larger for deeper lakes.

All of these properties can be rationalized by studying seasonal cycles of the shallow and deep lakes in their cold and warm regimes (**Fig. 5**). Throughout most of the cold season, the lake water remains vertically mixed throughout the whole column for shallower lakes and over the depths exceeding 100 m or more for deeper lakes (see, for example, Assel 1986). Hence, a deeper lake has a larger thermal inertia and it takes more forcing (and colder free-atmosphere temperatures) to cool it down to freezing

temperature and form ice in winter, explaining the property (i) above.

Properties (ii) and (iii) also have to do with a larger effective thermal inertia of deep lakes vs. that of the shallow lakes, albeit not quite as directly as the property (i). The ultimate reason behind (ii) and (iii) is that shallower lakes exhibit a longer stratified season in summer than deeper lakes (see Fig. 5). This is due, in turn, to an earlier onset of the spring overturn (which happens when the surface temperature reaches the value of 3.98°C corresponding to the largest density of water) in shallow regions of the lakes. By contrast, deeper lake columns have more water to mix, so the vertical density profile of a deeper lake remains nearly homogeneous and its surface temperature remains just below the maximum density threshold of 3.98°C longer than that of a shallower lake. An earlier spring overturn and an earlier formation of the summertime surface mixed layer in shallow lake areas is also a feature of the observed seasonal cycles of the lakes (not shown).

A typical depth of the summertime surface mixed layer of the Great Lakes is 10–20 m, so this layer’s thermal inertia is really small (see, for example, Assel 1986; McCormick 1998), and it responds to the atmospheric forcing fairly quickly. A longer duration of the summertime stratified season in shallower lakes thus translates to a longer time to efficiently alleviate the differences in the maximum summertime temperature between the cold and warm regimes — which dynamically originate earlier, in the cold season, due to workings of the ice–albedo feedback — via radiation and sensible/latent heat loss to the atmosphere [property (iii)]. Property (ii) is a byproduct of property (iii): the smaller the temperature ‘gap’ between the two regimes is, the smaller is the range of free-atmosphere temperature $T_{\max} - T_{\min}$ in which these regimes coexist.

The consequence of properties (ii) and (iii) is that shallower lakes transition from one regime to the other more easily than deeper lakes in response to forcing. In particular, under the action of atmospheric noise with amplitude between the temperature ‘gap’ values $T_{\max} - T_{\min}$ characterizing a shallow lake and a deep lake, the regime behavior of the shallow lake may not be immediately apparent as the temperature ‘trajectory’ would wander chaotically between the two regimes. On the other hand, the deep lake in this case would be characterized by quasi-stable regime behavior, possibly with occasional and easily identifiable transitions between the two regimes. These properties help explain amplification of the surface warming trends of deeper lakes vs. shallower lakes in the presence of global warming and atmospheric noise (see section 5).

4 Multiple regimes in three-column lakes

In this section, we study the behavior of three-column lakes (Fig. 3) whose bathymetry characteristics are chosen to approximate some of the Great Lakes (**Table 1**). Lake 1 is the deepest lake whose average depth approximates that of Lake Superior, Lake 3 (“Erie”) is the shallowest, and Lake 2 (“Michigan”) has an intermediate depth. The \overline{SW} forcing parameters [see Eq. (1)] for these lakes — 175 W m^{-2} (Lake 1), 190 W m^{-2} (Lake

2), and 195 W m^{-2} (Lake 3) — are also roughly comparable to the amounts of long-term mean shortwave radiation over Lakes Superior, Michigan, and Erie.

Figure 6 (left) presents the hysteresis curves of the deepest column of Lake 2 computed in the same way as for the one-column lake of section 3 (Fig. 4). Similar to the case of single-column lakes in Fig. 4, the Lake-2 three-column model without the ice–albedo effect does not have multiple climate regimes. By contrast, the full version of three-column model in which the ice albedo is much higher than that of the open water can have up to three different climate regimes for certain values of \bar{T} : the cold regime in which ice covers the entire lake surface during winter, the intermediate regime with ice covering only the intermediate-depth and the shallowest lake columns during winter, and the warm regime with only the shallowest lake column covered with ice in winter. The three sets of hysteresis curves in Fig. 6 (right) show the maximum (summertime) temperature for the three columns: the deepest (black), intermediate-depth (cyan) and the shallowest column (red), as a function of \bar{T} .

The bifurcation diagram for the shallowest Lake-3 model (**Fig. 7**) is qualitatively different from that for Lake 2 in that the regime transitions are spread out along the \bar{T} axis, and we do not find a range of \bar{T} in which more than two regimes coexist. The three sets of regime transitions in this case correspond to the transitions of the deepest, intermediate-depth, and shallowest lake columns from their respective wintertime ice-covered to perennially ice-free states, respectively. The \bar{T} thresholds for this transition are the lowest (-0.4°C , -0.2°C) for the deepest lake column, intermediate (1.4°C , 2.4°C) for the intermediate-depth column and the highest (2.4°C , 2.6°C) for the shallowest lake column; this is consistent with the property (i) of section 3. Furthermore, the gaps between maximum (summertime) temperature of warmer-vs.-colder regimes within each regime pair are in general much smaller than for the Lake-2 regimes, in accord with property (iii) of the one-column models in section 3. Note, however, that the relative sizes of these gaps are not merely the function of the lake depth, as in one-column models, but also depend on the relative areas of the lake columns (Table 1) and the efficiency of the horizontal atmospheric heat transport (not shown).

In summary, while the regime structure of the three-column lakes is more complex than that of flat-bottom lakes, the properties of the regimes and, in particular, their dependence on the lake depth in the two cases, are consistent.

5 Response of lakes to global warming

a) Lacustrine regional amplification of global warming. The bifurcation diagrams of the previous section were obtained by adding linear trends to the annual-mean free-atmosphere temperature \bar{T} . We now examine the evolution of three-column lake models under such warming trend (of 0.04°C per year) to gain insight into how the lake dynamics may amplify global warming on a regional scale. In the experiments of this section, we also added an idealized interannual variability on top of the linear global

warming signal in \bar{T} , by introducing alternating biennial anomalies of $\pm 2^\circ\text{C}$ to the \bar{T} time series. The standard deviation of the resulting interannual variability is similar to the observed variations (not shown).

For each of our three idealized lake models, we started with atmospheric conditions cold enough to freeze the entire lake in winter, and followed the evolution of the lakes' seasonal cycle in a long global-warming simulation set up as described above. We then computed the slopes of linear trends in the annual-mean lake-surface temperature for each lake column over the 20-yr sliding window. The resulting values of the maximum warming rates are listed in **Table 2**. Note that these warming trends all exceed the global warming rate of 0.04°C per year, are largest for the deepest Lake 1 and smallest for the shallowest Lake 3, in accordance with observations (section 1). We also recover the observed correlation between lake-column depth and surface warming rates within each lake, with the deepest lake columns exhibiting the largest warming rates.

The latter properties in our global warming experiments stem from the fact that the peak warming rates of the lakes arise due to transitions between the lake regimes, as cold regimes are gradually becoming less and less likely under the global warming. The peak differences between cold and warm regimes of deep lakes are larger than those between the regimes of shallow lakes (see sections 3 and 4); hence, deep lakes tend to exhibit larger warming rates. Furthermore, since the dynamical inertia of the shallow lakes is smaller, they are more likely to transition back and forth between their cold and warm regimes due to interannual atmospheric variability compared to the deep lakes. These multiple transitions smear out the peak warming rates of shallow lakes even further.

b) Discontinuous behavior of deep lakes. Finally, we present, in **Fig. 8**, an example of simulation with our Lake 2 forced by a combination of linear global warming trend in \bar{T} and random Gaussian noise in both \bar{T} and \overline{SW} , with the standard deviations of 2°C and 6 W m^{-2} , respectively; these values are consistent with observations of atmospheric interannual variability. The lake starts from the cold regime at low values of \bar{T} and. As \bar{T} gradually warms, the lake starts to transition back and forth between its colder and warmer regimes before arriving permanently to its final warm state. In the first half of the time series, the lake's cold regime is preferred, with the lake only experiencing occasional transitions to the warm regime for one or two years (where the minimum temperature remains above freezing throughout the year). In the second half of the time series though, the situation is completely reversed, with the warm regime being clearly dominant (ice only reappears in this column twice after the simulation year 90). This simulation qualitatively mimics the behavior of Lake Superior. Prior to 1997, this lake's climate was dominated by cold regime with an extensive wintertime ice cover (maximum $> 80\%$) and low summertime temperatures. After 1998, the lakes switched to the warm regime with maximum ice cover $< 60\%$ and warm lake temperature in summer: during this period, the lake's cold regime appeared three times, in years 2003, 2009, and 2014–15, but neither of these occurrences lasted more than two years.

The multiple stochastically forced transitions introduce an apparent decadal variability in the lake-temperature time series, consistent with the interannual memory of deep lakes, and 'diffuse' the lake warming to occupy a longer time interval. Still, note the jump-like

character of the lake-temperature time series in Fig. 8, with a clear step-like increase in maximum summertime water temperature around year 88 of simulation (equivalent to year 1998 in the case of the observed Lake Superior transition to its warm regime). By contrast, the time series of surface-water temperatures of shallower lakes exhibit less clear regime transitions (not shown), due to their smaller thermal and dynamical inertia. Hence, we expect the discontinuous regime behavior to be most pronounced for the deepest lakes like Lake Superior, and less so for shallower lakes.

6 Conclusions

The main result of the present study is that nonlinear dynamics operating in our coupled lake–ice–atmosphere model allow us to faithfully simulate large amplification of the global warming signal in deep-lake areas, as was observed in the Great Lake region during recent decades. These dynamics manifest in the existence of multiple regional climate regimes of the lakes — that is, distinct seasonal cycles of the lakes, with warmer or colder summertime temperatures and less or more extensive wintertime ice cover, — arising under the identical seasonally varying forcing. The persistence characteristics and sheer differences between the regimes depend on the depth of the lake. Deep lakes, which have a large thermal/dynamical inertia, exhibit large differences between the regimes and are resilient to external perturbations, whereas the differences between shallow-lake regimes are less pronounced, and the transitions between them under interannual atmospheric variability are easier to achieve. Hence, the deep lakes exhibit a stronger — often jump-like — response to global warming forcing as they undergo changes toward a state in which their warmer regimes gradually become progressively more likely, consistent with observations.

The regimes in our model only occur in the presence of the ice–albedo feedback nonlinearity; therefore, our results corroborate Austin and Colman’s (2007) original hypothesis about the central role of this feedback in the accelerated warming of Lake Superior. Our hypothesis of nonlinear regime dynamics behind the lacustrine regional amplification of global warming is, however, novel, and complements a rich spectrum of existing theories (see section 1). Sorting out relative contributions to the lake warming from a large suite of possible linear and nonlinear mechanisms will require further work.

Nonlinear regimes due to ice–albedo feedback have been studied before in a variety of climatic problems, including that of glacial-to-interglacial transitions which involve land-ice and sea-ice feedbacks, as well as in addressing a possibility of abrupt changes in Arctic sea ice under climate change (see Merryfield et al. 2008 for a review). Our present study revisits this concept in a novel context of the regional climate change and provides a new framework for assessing and understanding climatic effects of mid-latitude lakes.

Acknowledgements. We thank Michael Notaro, Stephen Vavrus and Yafang Zhong for numerous valuable discussions. This work was supported by the NSF grant 1236620.

References

- Ackerman S, Heidinger A, Foster M, Maddux B (2013) Satellite regional cloud climatology over the Great Lakes. *Remote Sensing* 5: 6223–6240
- Alexander MA, Penland C (1996) Variability in a mixed layer ocean model driven by stochastic atmospheric forcing. *J Clim* 9: 2424–2442
- Arvola L, George G, Livingstone DM, Jarvinen M, Blenckner T, Dokulil MT, Jennings E, Aonghusa CN, N'ogues P, Noges T, Weyhenmeyer GA (2010) The impact of the changing climate on the thermal characteristics of lakes. In: George G (ed) *The Impact of Climate Change on European Lakes*. Aquatic Ecology Series, pp 85–101, Springer, Netherlands
- Assel R (1986) Fall and winter thermal structure of Lake Superior. *J Great Lakes Res* 12:(4) 251–262
- Austin J, Allen J (2011) Sensitivity of summer Lake Superior thermal structure to meteorological forcing. *Limnol Oceanogr* 56: 1141–1154
- Austin JA, Colman SM (2007) Lake Superior summer water temperatures are increasing more rapidly than regional air temperatures: A positive ice-albedo feedback. *Geophys Res Lett* 34: L06604
- Bennington V, Notaro M, Holman KD (2014) Improving climate sensitivity of deep lakes within a regional climate model and its impact on simulated climate. *J Clim* 27: 2886–2911
- Byrne MP, O’Gorman PS (2012) Land–ocean warming contrast over a wide range of climates: Convective quasi-equilibrium theory and idealized simulations. *J Clim* 26: 4000–4016
- Dake, JMK., Harleman DRF (1969) Thermal stratification in lakes: Analytical and laboratory studies. *Water Resour Res* 5: 484–495
- De Boyer Montegut C, Madec G, Fischer AS, Lazar A, Iudicone D (2004) Mixed layer depth over the global ocean: An examination of profile data and a profile-based climatology. *J Geophys Res* 109: C12003, doi:10.1029/2004JC002378
- Desai AR, Austin JA, Bennington V, McKinley GA (2009) Stronger winds over a large lake in response to weakening air-to-lake temperature gradient. *Nature Geoscience* 2: 855–858
- Fang X, Stefan HG (1998) Temperature variability in lake sediments. *Water Resour Res* 34: 717–729, doi:10.1029/97WR03517
- Fink G, Schmid M, Wahl B, Wolf T, Wuest A (2014) Heat flux modifications related to climate-induced warming of large European lakes. *Water Resour Res* 50: 2072–2085
- Foster M, Heidinger A (2013) PATMOS-x: Results from a diurnally corrected 30-yr satellite cloud climatology. *J Clim* 26: 414–425
- Frankignoul C, and Hasselmann K (1977) Stochastic climate models. Part II: Application to sea-surface temperature anomalies and thermocline variability. *Tellus* 29: 289–305

- Gerbush M, Kristovich D, Laird N (2008) Mesoscale boundary layer and heat flux variations over pack ice-covered Lake Erie. *J Appl Meteor Clim* 47: 668–682.
- Gronewold AD, Anderson EJ, Lofgren B, Blanken PD, Wang J, Smith J, Hunter T, Lang G, Stow CA, Beletsky D, Bratton J (2015) Impacts of extreme 2013–2014 winter conditions on Lake Michigan’s fall heat content, surface temperature, and evaporation. *Geophys Res Lett* 42: 3364–3370
- Hakanson L (1995) Models to Predict Secchi Depth in Small Glacial Lakes. *Aquat Sci* 57: 31–53
- Hampton SE, Izmet’eva LR, Moore MV, Katz SL, Dennis B, Silow EA (2008) Sixty years of environmental change in the world’s largest freshwater lake—Lake Baikal, Siberia. *Global Change Biol* 14:(8) 1947–1958, doi:10.1111/j.1365-2486.2008.01616.x
- Hanrahan, JL, Kravtsov S, Roebber PJ (2010) Connecting past and present climate variability to the water levels of Lake Michigan and Huron. *Geophys Res Lett* 37: L01701
- Heggen RJ (1983) Thermal dependent properties of water. *J Hydraul Eng* 109: 298–302
- Henderson-Sellers B (1986) Calculating the surface energy balance for lake and reservoir modeling: A review. *Rev Geophys* 24: 625–649
- Hostetler S, Bartlein PJ (1990) Simulation of lake evaporation with application to modeling lake-level variations at Harney-Malheur Lake, Oregon. *Water Resour Res* 26: 2603–2612.
- Joshi MM, Gregory JM (2008) Dependence of the land–sea contrast in surface climate response on the nature of the forcing. *Geophys Res Lett* 35: L24802
- Joshi MM, Gregory JM, Webb MJ, Sexton DMH, John TC (2008) Mechanism for the land/seawarming contrast exhibited by simulations of climate change. *Clim Dyn* 30: 455–465
- Kara AB, Rochford PA, Hurlburt HE (2000) An optimal definition for ocean mixed layer depth. *J Geophys Res* 105: 16803–16821
- Lau N-C, Nath MJ (1996) The role of the “atmospheric bridge” in linking tropical Pacific ENSO events to extratropical SST anomalies. *J Clim* 9: 2036–2057
- Long CNE, Dutton EG, Augustine JA, Wiscombe W, Wild M, McFarlane SA, Flynn CJ (2009) Significant decadal brightening of downwelling shortwave in the continental United States. *J Geophys Res* 114: D00D06, doi:10.1029/2008JD011263.
- Magnuson JJ (2000) Historical trends in lake and river ice cover in the Northern Hemisphere. *Science* 289: (5485) 1743–1746, doi:10.1126/science.289.5485.1743
- Manabe S, Stouffer RJ, Spelman MJ, Bryan K (1991) Transit responses of a coupled ocean–atmosphere model to gradual changes of atmospheric CO₂. Part I: Annual mean response. *J Clim* 4: 785–818
- Mantua NJ, Zhang Y, Wallace JM, Francis RC (1997) A Pacific interdecadal climate oscillation with impacts on salmon production. *Bull Amer Meteor Soc* 78: 1069–1079

- Martynov A, Sushama L, Laprise R (2010) Simulation of temperate freezing lakes by one-dimensional lake models: Performance assessment for interactive coupling with regional climate models. *Bor Environ Res* 15: 143–164
- McCormick MJ, Meadows GA (1988) An intercomparison of four mixed layer models in a shallow inland sea. *J Geophys Res* 93: 6774–6788
- Merryfield WJ, Holland MM, Monahan AH (2008) Multiple equilibria and abrupt transitions in Arctic summer sea ice extent. In: DeWeaver ET, Bitz CM, Tremblay L-B (eds). *Arctic Sea Ice Decline: Observations, Projections, Mechanisms, and Implications*, doi: 10.1029/180GM11, pp. 151–174
- O'Reilly CM, Sharma S, Gray DK, Hampton SE, et al. (2015) Rapid and highly variable warming of lake surface waters around the globe. *Geophys Res Lett* 42: 10773–10781, doi:10.1002/2015GL066235
- Piccolroaz S, Toffolon M, Majone B (2015) The role of stratification on lakes' thermal response: The case of Lake Superior. *Water Resour. Res.* 51, doi:10.1002/2014WR016555
- Prinsenberg S., Peterson IK (2002) Variations in air-ice drag coefficient due to ice surface roughness. *Inter J Offshore Polar Eng* 12: (2), ISSN 1053–5381
- Ryan PJ, Harleman DRF (1971) Prediction of the annual cycle of temperature changes in a stratified reservoir: Mathematical model and user's manual. Technical Report 137, Massachusetts Institute of Technology.
- Schneider P, Hook SJ (2010) Space observations of inland water bodies show rapid surface warming since 1985. *Geophys Res Lett* 37: L22405
- Schneider P, Hook SJ, Radocinski RG, Corlett GK, Hulley GC, Schladow SG, Steissberg TE (2009) Satellite observations indicate rapid warming trend for lakes in California and Nevada. *Geophys Res Lett* 36: L22402, doi:10.1029/2009GL040846
- Semtner AJ (1976) A model for the thermodynamic growth of sea ice in numerical investigations of climate. *J Phys Oceanogr* 6: 379–389
- Subin ZM, Riley WJ, Mironov D (2012) An improved lake model for climate simulations: Model structure, evaluation, and sensitivity analyses in CESM1. *J Adv Mod Earth Sys* 4: M02001, doi:10.1029/2011MS000072
- Sutton RT, Dong B, Gregory MG (2007) Land/sea warming ratio in response to climate change: IPCC AR4 model results and comparison with observations. *Geophys Res Lett* 34: L02701
- Toffolon M, Piccolroaz S, Majone B, Soja A, Peeters F, Schmid M, Wuëst A (2014) Prediction of surface temperature in lakes with different morphology using air temperature. *Limnol Oceanogr* 59: (6) 2185–2202.
- Van Cleave K, Lenters JD, Wang J, Verhamme EM (2014) A regime shift in Lake Superior ice cover, evaporation, and water temperature following the warm El Niño winter of 1997–1998. *Limnol Oceanogr* 59: (6) 1889–1898, doi:10.4319/lo.2014.59.6.1889

Vavrus S, Wynne R, Foley J (1996) Measuring the sensitivity of southern Wisconsin lake ice to climate variations and lake depth using a numerical model. *Limnol Oceanogr* 41: 822–831

Zhong Y, Notaro M, Vavrus SJ (2016) Recent accelerated warming of the Laurentian Great Lakes: Physical drivers, *Limnol Oceanogr*, doi: 10.1002/lno.10331

Table captions

Table 1: Geometry of three-column lake models. Lake 1 mimics Lake Superior, Lake 2 — Michigan and Lake 3 — Erie.

Table 2: The peak warming trends ($^{\circ}\text{C}$ per year) in the annual-mean surface-water temperature for the three idealized lake models from Table 1 subjected to the linear trend of 0.04 $^{\circ}\text{C}$ per year plus a periodic interannual variability: see text for details. The warming trends were computed using the 20-yr moving-window linear least-square trends of lake-surface temperature.

Figure captions

Fig. 1: The 1995–2012 warming trend in the annual-mean surface water temperature versus water depth for Great Lakes. The trends were spatially averaged over the areas of a given depth within each lake (see panel captions). These results are based on the satellite observations of surface temperature from the Great Lakes Surface Environmental Analysis (GLSEA) operated by NOAA’s Great Lakes Environmental Research Laboratory (GLERL).

Fig. 2: A simulation of temperature ($^{\circ}\text{C}$) below buoy station 45002 in northern Lake Michigan, for the year 1996. The purple stripes correspond to the regions where temperature is $3.98 \pm 0.05^{\circ}\text{C}$. The vertical grid spacing is 5 m.

Fig. 3: Geometry of the coupled model with three-column lake component. Top panel: cross-section; bottom panel: plan view.

Fig. 4: The hysteresis diagrams in the phase plane of maximum (summertime) surface water temperature for the lakes of different depths (see panel captions) and the concurrent annual-mean lower free atmosphere’s temperature forcing \bar{T} . The blue curves indicate the evolution of maximum surface water temperature when \bar{T} slowly warms at the rate of $+0.04^{\circ}\text{C}$ per year. The red curves indicate the evolution of maximum surface water temperature when \bar{T} slowly cools at the rate of $+0.04$ $^{\circ}\text{C}$ per year. The ice albedo is at the default value of 0.45. For comparison, the green curves show the results of simulations with the ice albedo set to the water albedo of 0.05, which exhibit no difference between the slow warming and slow cooling results. Units are $^{\circ}\text{C}$.

Fig. 5: Seasonal cycle of lake temperature in °C for the 100-m-deep lake (left column) and 50-m-deep lake (right column). Top row: cold regime; bottom row: warm regime. The purple stripes correspond to the regions where temperature is $3.98 \pm 0.05^\circ\text{C}$.

Fig. 6: Left: The hysteresis diagram in the phase plane of maximum (summertime) surface water temperature for the deepest column of Lake 2 and the concurrent annual-mean free-atmosphere temperature forcing \bar{T} . We consider two cases: simulations with the ice albedo at the default value of 0.45 (black) and simulations with the ice albedo set to the water albedo of 0.05 (green). Units are °C. This figure is analogous to Fig. 4 for the one-column lake model. Right: The hysteresis diagrams of maximum (summertime) surface water temperature for Lake-2 model's deep (black), intermediate (cyan) and shallow (red) columns, shown together. The ice albedo here is at the default value of 0.45.

Fig. 7: Top: The hysteresis diagrams of maximum (summertime) surface water temperature for Lake-3 model's deep (black), intermediate (cyan) and shallow (red) columns. This figure is analogous to Fig. 6 (right).

Fig. 8: A realization of the "global warming" experiment (forced by the steady 0.04°C per year trend in the upper-air annual-mean temperature \bar{T}) with superimposed atmospheric stochastic forcing for Lake 2. Shown are the time series of the maximum (green) and minimum (blue) surface water temperatures of the deepest column of Lake 2.

Table 1: Geometry of three-column lake models. Lake 1 mimics Lake Superior, Lake 2 — Michigan and Lake 3 — Erie.

Lake 1	Depth (m)	Fractional area
Column 1	50	0.1
Column 2	150	0.5
Column 3	225	0.3
Land	—	0.1

Lake 2	Depth (m)	Fractional area
Column 1	30	0.2
Column 2	80	0.5
Column 3	140	0.2
Land	—	0.1

Lake 3	Depth (m)	Fractional area
Column 1	15	0.4
Column 2	20	0.4
Column 3	40	0.1
Land	—	0.1

Table 2: The peak warming trends ($^{\circ}\text{C}$ per year) in the annual-mean surface-water temperature for the three idealized lake models from Table 1 subjected to the linear trend of 0.04°C per year plus a periodic interannual variability: see text for details. The warming trends were computed using the 20-yr moving-window linear least-square trends of lake-surface temperature.

Warming-trend	Shallow column	Intermediate column	Deep column	Overall
Lake 1	0.137	0.171	0.183	0.171
Lake 2	0.090	0.119	0.129	0.116
Lake 3	0.063	0.085	0.092	0.076

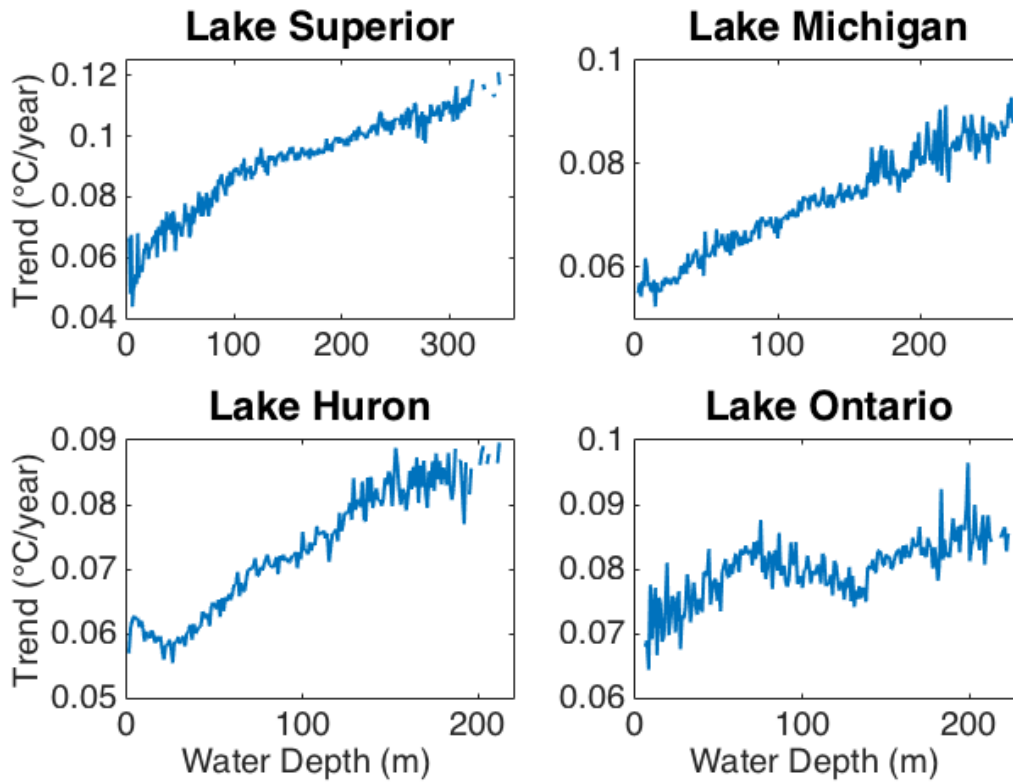


Fig. 1: The 1995–2012 warming trend in the annual-mean surface water temperature versus water depth for Great Lakes. The trends were spatially averaged over the areas of a given depth within each lake (see panel captions). These results are based on the satellite observations of surface temperature from the Great Lakes Surface Environmental Analysis (GLSEA) operated by NOAA’s Great Lakes Environmental Research Laboratory (GLERL).

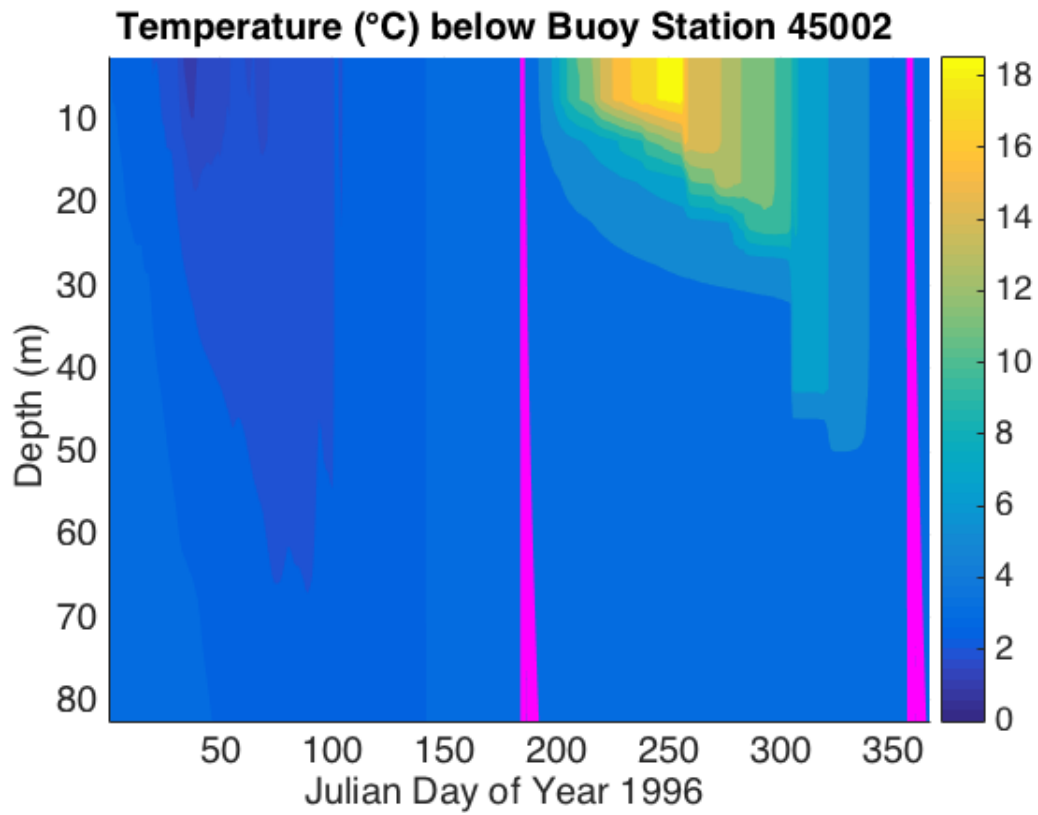


Fig. 2: A simulation of temperature (°C) below buoy station 45002 in northern Lake Michigan, for the year 1996. The purple stripes correspond to the regions where temperature is $3.98 \pm 0.05^\circ\text{C}$. The vertical grid spacing is 5 m.

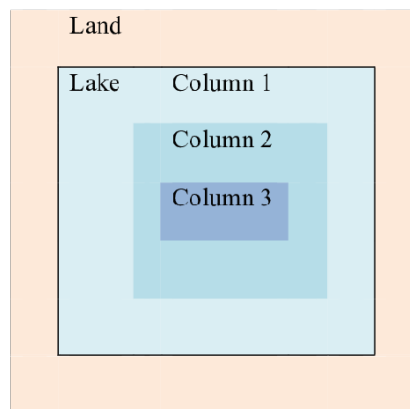
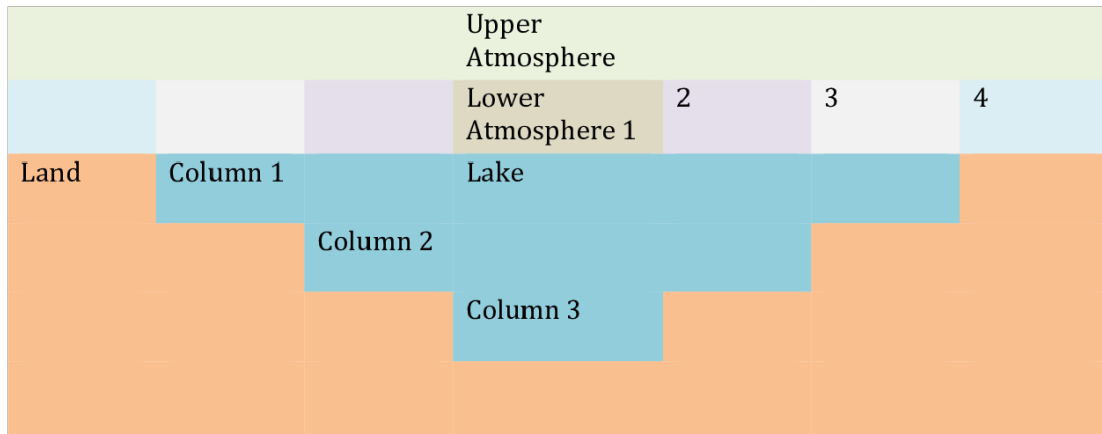


Fig. 3: Geometry of the coupled model with three-column lake component. Top panel: cross-section; bottom panel: plan view.

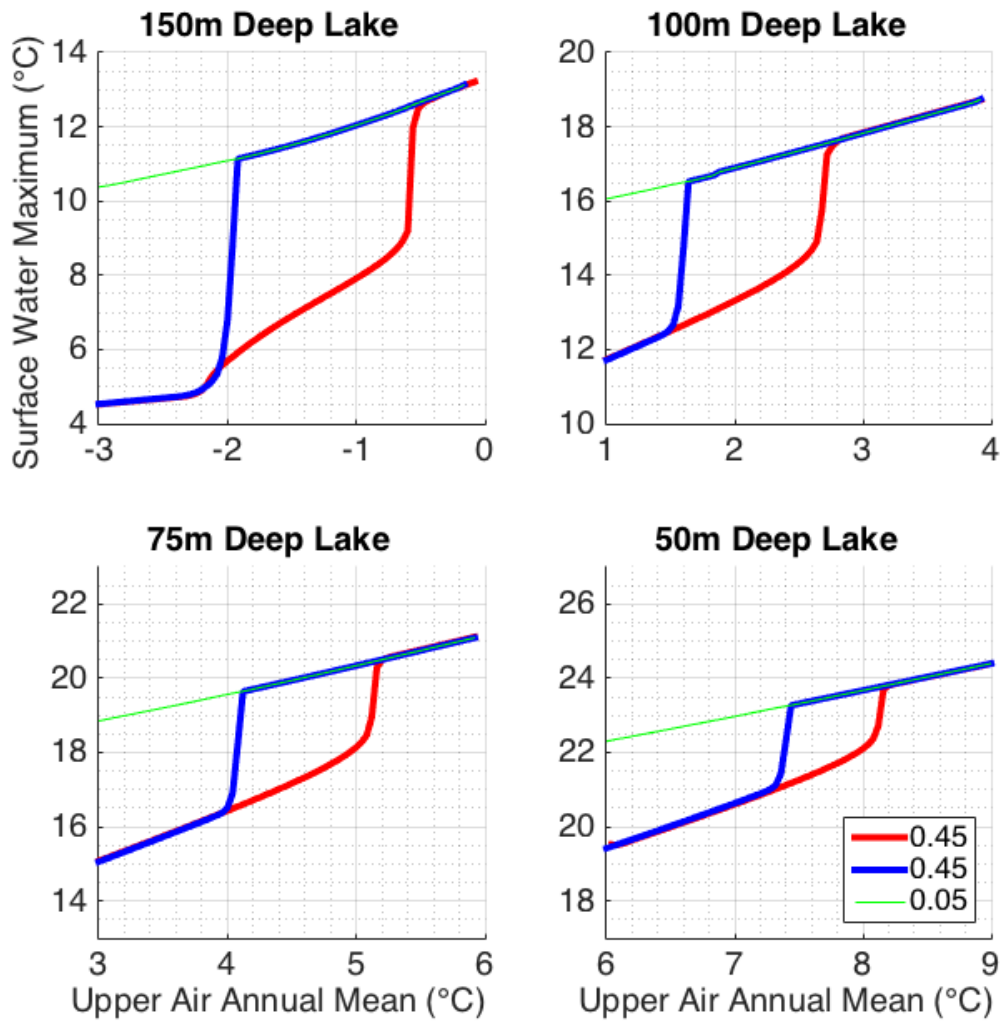


Fig. 4: The hysteresis diagrams in the phase plane of maximum (summertime) surface water temperature for the lakes of different depths (see panel captions) and the concurrent annual-mean lower free atmosphere's temperature forcing \bar{T} . The blue curves indicate the evolution of maximum surface water temperature when \bar{T} slowly warms at the rate of $+0.04^\circ\text{C}$ per year. The red curves indicate the evolution of maximum surface water temperature when \bar{T} slowly cools at the rate of $+0.04^\circ\text{C}$ per year. The ice albedo is at the default value of 0.45. For comparison, the green curves show the results of simulations with the ice albedo set to the water albedo of 0.05, which exhibit no difference between the slow warming and slow cooling results. Units are $^\circ\text{C}$.

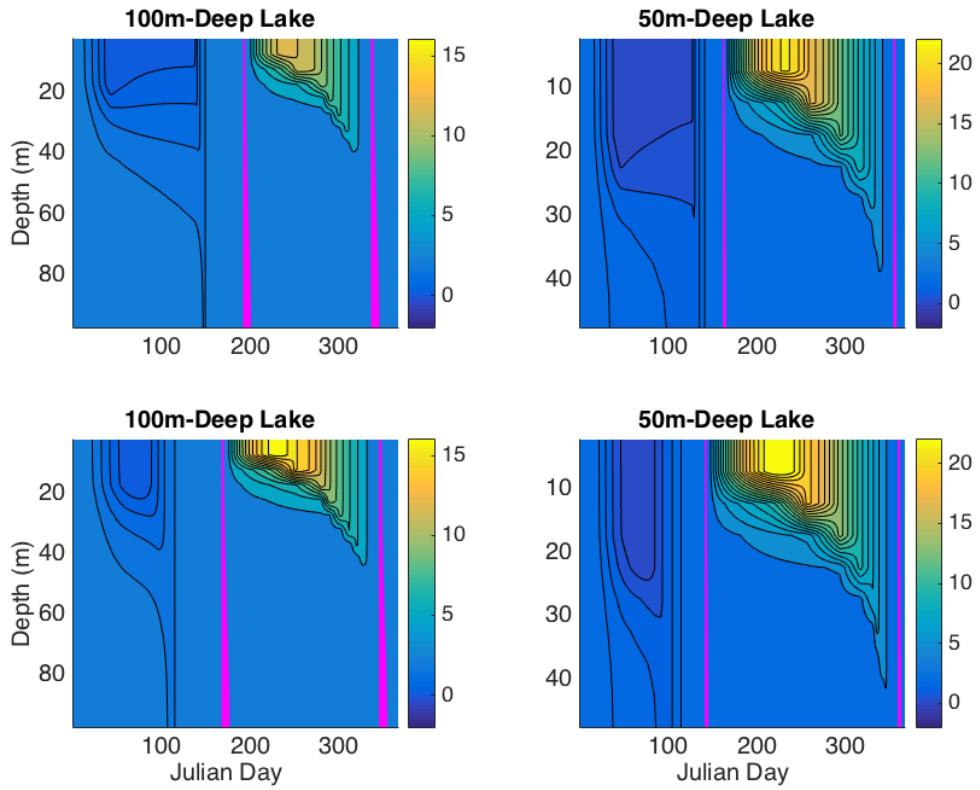


Fig. 5: Seasonal cycle of lake temperature in °C for the 100-m-deep lake (left column) and 50-m-deep lake (right column). Top row: cold regime; bottom row: warm regime. The purple stripes correspond to the regions where temperature is $3.98 \pm 0.05^\circ\text{C}$.

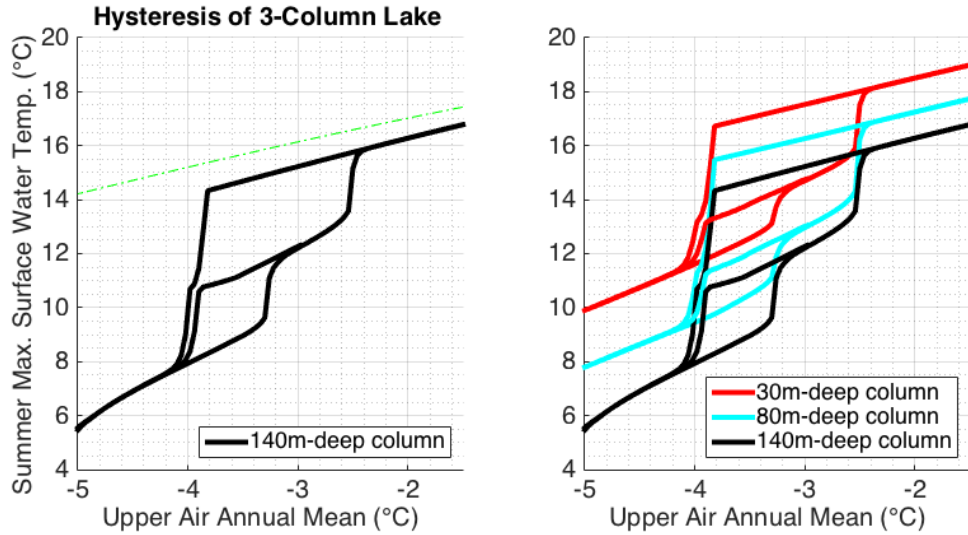


Fig. 6: Left: The hysteresis diagram in the phase plane of maximum (summertime) surface water temperature for the deepest column of Lake 2 and the concurrent annual-mean free-atmosphere temperature forcing \bar{T} . We consider two cases: simulations with the ice albedo at the default value of 0.45 (black) and simulations with the ice albedo set to the water albedo of 0.05 (green). Units are °C. This figure is analogous to Fig. 4 for the one-column lake model. Right: The hysteresis diagrams of maximum (summertime) surface water temperature for Lake-2 model's deep (black), intermediate (cyan) and shallow (red) columns, shown together. The ice albedo here is at the default value of 0.45.

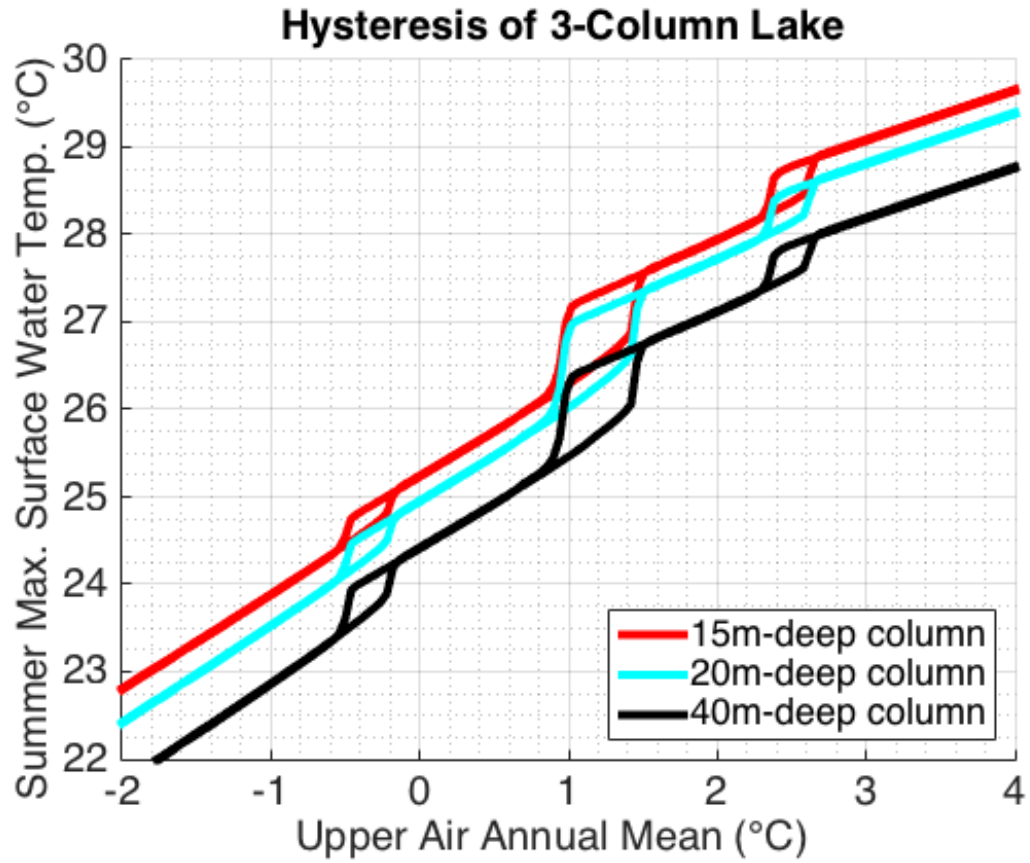


Fig. 7: Top: The hysteresis diagrams of maximum (summertime) surface water temperature for Lake-3 model's deep (black), intermediate (cyan) and shallow (red) columns. This figure is analogous to Fig. 6 (right).

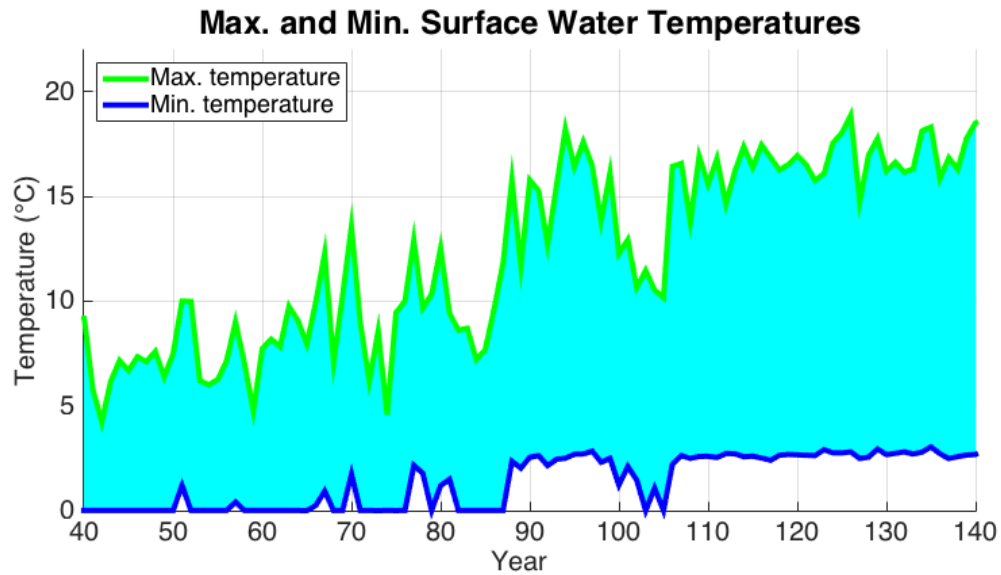


Fig. 8: A realization of the "global warming" experiment (forced by the steady 0.04°C per year trend in the upper-air annual-mean temperature \bar{T}) with superimposed atmospheric stochastic forcing for Lake 2. Shown are the time series of the maximum (green) and minimum (blue) surface water temperatures of the deepest column of Lake 2.